Journal of Hydrology 563 (2018) 766–777

Contents lists available at ScienceDirect

Journal of Hydrology

journal homepage: www.elsevier.com/locate/jhydrol

Research papers

# Hydroclimatic response of evapotranspiration partitioning to prolonged droughts in semiarid grassland

Dongmei Han[a], Guoqiang Wang[a,*], Tingxi Liu[b], Bao-Lin Xue[a,*], George Kuczera[c], Xinyi Xu[a]

[a] College of Water Sciences, Beijing Normal University, Beijing 100875, China
[b] College of Water Conservancy and Civil Engineering, Inner Mongolia Agricultural University, Hohhot, Inner Mongolia Autonomous Region 010018, China
[c] School of Engineering, University of Newcastle, Callaghan, NSW 2308, Australia

ARTICLE INFO

This manuscript was handled by G. Syme, Editor-in-Chief, with the assistance of Ashok Mishra, Associate Editor

*Keywords:*
Semiarid grassland
Water fluxes
ET partitioning
Underlying water use efficiency (uWUE)
Prolonged drought

ABSTRACT

A warming climate is expected to perturb the hydrological cycle, resulting in changes to both the frequency and duration of drought, especially in arid and semiarid grassland. Although considerable attention has been paid to the responses of key water fluxes to severe drought, few have explored the effects of prolonged drought on evapotranspiration (ET), its partitioning into vegetation transpiration (T) and soil evaporation (E), and its relationship with vegetation productivity. In this study, we used a combination of the eddy covariance (EC) flux technique and satellite remote sensing products to evaluate the effects of prolonged drought on ET components based on the concept of underlying water use efficiency (uWUE). The results showed T accounted for about 51% (standard deviation ± 0.03%) of ET during prolonged drought lower than those in normal and/or wet years (range, 59–62%). We detected strong positive relationships between the T/ET ratios and aboveground biomass (AGB), leaf area index (LAI), and precipitation ($R^2$ of 0.80, 0.58, and 0.49, respectively). The specific responses of ecosystem functioning to prolonged drought indicated that grassland ecosystem was able to resist the drought disturbance and retain vegetation growth to a certain extent unless extreme drought hit. The results implied that more intense and prolonged droughts will result in ecological degradation and substantial changes in ecosystem functioning. And these results improve our understanding of how the climate change will affect the function and structure of grassland ecosystem.

## 1. Introduction

Analyses of precipitation, streamflow, and soil moisture have shown a trend of increasing drought in the 21st century (Dai, 2011a,b). More intense and persistent droughts are projected to cause major shifts in key processes in the water cycle, which in turn will affect the carbon and nitrogen cycles in terrestrial ecosystems (Coners et al., 2016). Poncecampos et al. (2013) suggested that large regions have become more arid, starting with water-limited, low-productivity grasslands. Grasslands are the main vegetation type in semi-arid regions of China, and are ecologically fragile and sensitive to climatic changes and anthropogenic disturbances (Li et al., 2007). Additionally, grasslands supply numerous ecosystem service functions and have been recognized as the most significant ecological barriers in North China. Therefore, grassland ecosystems, especially those in arid and semiarid regions, have attracted growing attention from researchers (Sun et al., 2016).

Water fluxes were found to be the most crucial parameters influencing species composition and vegetation productivity in grassland ecosystems when drought-induced water limitations was severe (Wilske et al., 2010; Trenberth et al., 2014). Variations in water fluxes are in large part due to changes in evapotranspiration (ET), which is water loss via soil surface evaporation (E) and plant transpiration (T) (Fisher et al., 2008; Zhang et al., 2016). The difference between T and E is considerable, since the former is an ecohydrological link between the atmosphere and terrestrial ecosystems, and the latter is the direct process of water exchange between the soil surface and the atmosphere. Thus, partitioning ET into its two components may help us to understand the interaction mechanism between the land and atmosphere, and the key processes of water and energy balances between plants and the atmosphere (Lawrence et al., 2007; Zhou et al., 2016). Recent research on the impact of climate change on key elements in the water cycle has focused on the response of ET and vegetation growth to altered hydroclimatic conditions, largely to flash drought years (Milly and Dunne, 2016; Zhang and Liu, 2014). Climatic extremes occurring over multiple and consecutive years have accumulated non-linear effects on ecosystems that cannot be predicted from single-year events (Weaver and Albertson, 1939), since prolonged drought may cross ecological thresholds and threaten the inherent characteristics of ecosystems,

* Corresponding authors at: College of Water Sciences, Beijing Normal University, Xinjiekouwai Street 19, Haidian, Beijing 100875, China.
*E-mail addresses:* wanggq@bnu.edu.cn (G. Wang), xuebl@bnu.edu.cn (B.-L. Xue).

https://doi.org/10.1016/j.jhydrol.2018.06.048
Received 6 December 2017; Received in revised form 22 May 2018; Accepted 19 June 2018
Available online 21 June 2018
0022-1694/ © 2018 Elsevier B.V. All rights reserved.

resulting in biome reorganization (Poncecampos et al., 2013). However, our knowledge about the responses of ET partitioning to more intense and prolonged droughts, and about how to assess the factors that control ET partitioning, is still limited.

Recent findings suggested that model simulations coupled with the eddy covariance (EC) technique is the most direct and common method to partition the contributions of E and T to water loss (i.e., ET). The models used in recent studies include water and energy process-based models (e.g., the forest landscape productivity model, FLPM; the grassland landscape productivity model, GLPM) (Zhang and Liu, 2014), optimal partitioning (Berkelhammer et al., 2016), isotope partitioning (Berkelhammer et al., 2016), a bio-meteorological approach based on Priestley-Taylor (Fisher et al., 2008), the Penman-Monteith-Leuning (PML) model (Leuning et al., 2008), and the underlying water use efficiency (uWUE method, Zhou et al., 2014, 2016). Some models such as the FLPM model (or GLPM) and the stable isotope technique require the numerous complex parameters that rely on intensive field measurements, hence it remains the challenge to continuously measure ET components in field.

The uWUE method ($uWUE = GPP \cdot VPD^{0.5}/ET$) proposed by Zhou et al. (2014) is based on the relationships between ET and gross primary productivity (GPP) and vapor pressure deficit (VPD), and is considered as a relatively simple method to partition ET. The uWUE method is mainly based on the assumption that the maximum of water use efficiency (WUE) for a growing season is essentially constant over time for a given uniform ecosystem. This simple method of obtaining uWUE using available daily (summed from half-hourly measurements) FluxNet eddy covariance (EC) measurements has been used to calculate ET partitioning for various terrestrial ecosystems based on the relationship between $GPP \cdot VPD^{0.5}$ and ET.

Vegetation indexes (VIs) are effective indicators for exploring the interplay between climate change and vegetation growth (Pallett et al., 2016; Ren et al., 2017). The enhanced vegetation index (EVI) reflects the process of vegetation growth more exactly than does the normalized difference vegetation index (NDVI), which might reach its saturation value in the phase of maximum vegetation cover (Huete et al., 2002). Grassland biomass, especially aboveground biomass (AGB), is widely used to represent vegetation growth because of its close relationship with the carbon cycle and grassland productivity (Han et al., 2018; Hall et al., 2000). The AGB has been used to analyze the dynamics of vegetation growth at long-term and large spatial scales, where vegetation growth is estimated by a regression between field measurements and remote sensing data (Ren et al., 2017; Zhou et al., 2016). Numerous findings suggested that an inversion model between AGB and EVI derived from MODIS to estimate AGB has been commonly used, which can accurately reflect the variations in ecosystem functioning under altered hydroclimatic conditions (Todd et al., 1998; Méndez-Barroso et al., 2009).

Here, the main objectives of this study were: (1) to characterize the seasonal and interannual variations in droughts across the study area over the past 50 years, (2) to evaluate and correct the MODIS ET and GPP estimates against *in-situ* measurements, and to estimate the contribution of T to ET under prolonged droughts using the uWUE technique, and (3) to elucidate the factors controlling the T/ET ratio under prolonged drought.

## 2. Materials and methods

### 2.1. Study area

The study area is located in the northeast of Inner Mongolia, China with an area of $2.9 \times 10^5\,km^2$ (111°06′–121°03′E, 41°34′–50°13′N, Fig. 1a). It experiences a semiarid continental temperate climate, and receives 300–500 mm of annual precipitation with significant interannual variability. The growing season is generally from May to September when 80% of annual precipitation occurs. The mean temperature is within the range of −3.0 °C to 2 °C and the mean temperature of the growing season ranges from 20 °C to 38 °C. The main vegetation type is semiarid typical steppe, and *Leymus chinensis* and *Stipa baicalensis* are the dominant native species. The soil types are chernozem soil (GBT 17296-2009), black soil, and aeolian sandy soils. These are distributed across a wide range of elevations (average range: 400–1800 m above sea level, Fig. 1c). As reported by Sun et al. (2017), there are no significant differences in spatial patterns of climatic factors (including precipitation, and temperature) in the study area. Thus, the effect of elevation on spatial differences of temperature, precipitation and other climatic factors are not considered in our study. In the recent past, increases in the severity and frequency of hydroclimatic disturbances have changed the distribution pattern of hydrothermal conditions and the physicochemical properties of soil (Wang et al., 2014; Wang et al., 2015; Yang et al., 2014). These changes have profoundly influenced the function, structure and species composition of the grassland ecosystems in this area.

### 2.2. Sampling and meteorological data preparation

Aboveground biomass (AGB) and plant communities were surveyed and samples were collected from 75 sites (all in grassland) in early August in 2015, and from 55 sites (all in grassland) in early August in 2016 (Fig. 1a). We randomly assigned 3–5 samples (each from 1-$m^2$ plot) to every 50 km. The survey parameters recorded in each plot were the amount, coverage, height, and density of all plants, height and coverage of plant communities, and location (longitude, latitude, and altitude). In each sample, AGB was harvested at ground level from the two random 0.25 $m^2$ quadrats, and then dried to constant weight at 100 °C for ~12 h before measuring dry weight (Coyle et al., 2008). As shown in Fig. 1a, the number of sampling sites was sufficiently large to obtain an accurate value for AGB.

Daily meteorological data were collected from 13 meteorological stations around the study area (Fig. 1a). The data included precipitation (pre, mm), near-surface (2 m) air temperature (tem, °C), near-surface (2 m) wind speed (wind, $m \cdot s^{-1}$), near-surface (2 m) specific humidity (shum, %), and near-surface (2 m) pressure (pres, Pa). These data were obtained from the China Meteorological Data Service Center (http://data.cma.cn/site/index.html). Climate data covered the period from January 1961 to December 2015. For a small amount of missing data (< 1%), the average was calculated from data collected in other years at the same station. The daily data for each meteorological variable were summed to obtain monthly and annual data at the station level, and were further interpolated to generate a new dataset with 1-km spatial resolution using the inverse-distance weighting (IDW) method (Kurtzman et al., 2009). The interpolated meteorological values were averaged by all pixels, which was identical to those across the study area. The atmospheric vapor pressure deficit (VPD, kPa) was the difference between the saturated vapor pressure and the actual vapor pressure, which was calculated based on the Penman-Monteith (P-M) method using the above meteorological data (Vörösmarty et al., 1998).

### 2.3. In-situ flux data observation and processing

To obtain potential uWUE ($uWUE_p$) and to validate the remote sensing estimates, *in-situ* data from the NeiMengGu site (NMG) (43°32′N, 116°40′E) were collected from the ChinaFLUX network (http://www.chinaflux.org/) (Fig. 1a). The site is characterized as a *Leymus chinensis* ecological type in the temperature typical grassland of Inner Mongolia. It experiences a temperate and semiarid continental climate with mean annual precipitation of 350 mm and mean annual temperature of 0.9 °C. The dominant plant species are *Leymus chinensis*, *Stipa baicalensis*, *Cleistogenes squarrosa*, and *Agropyron cristatum*. The canopy height is approximately 50–60 cm and the vegetation coverage is 30%–40%. The observed dataset consisted of half-hourly air temperature (TA, °C), latent heat flux (LE, $W \cdot m^{-2}$), net ecosystem exchange

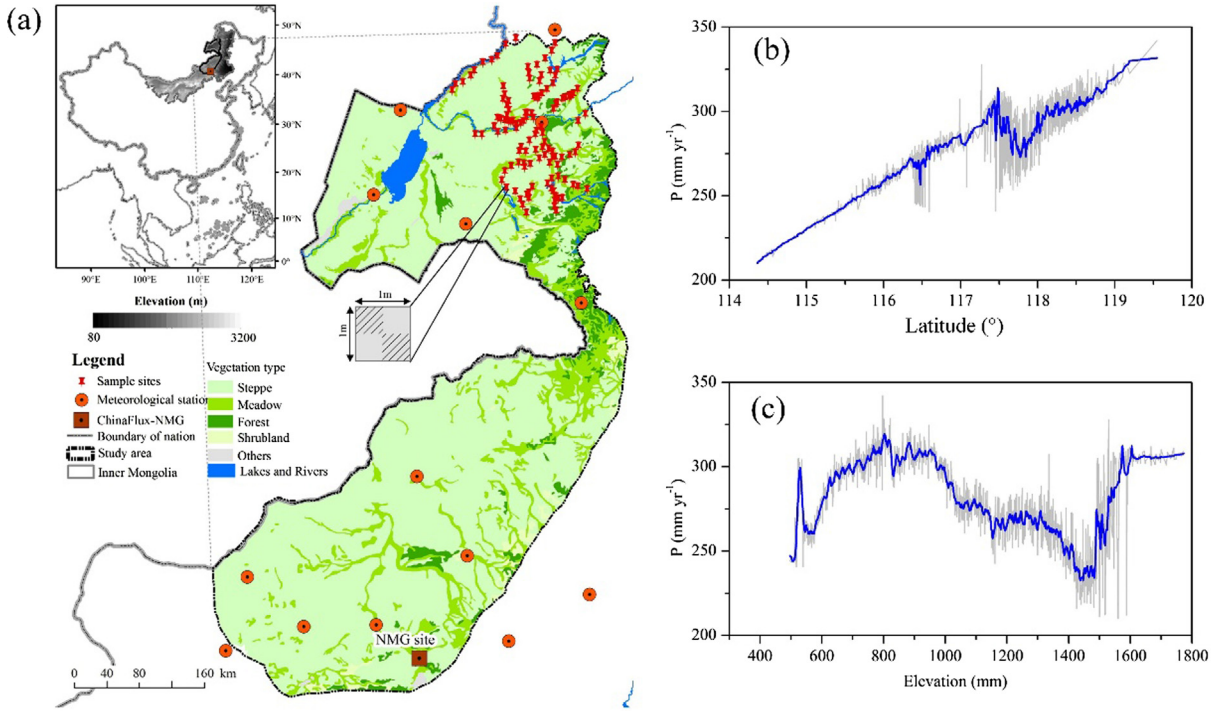


**Fig. 1.** (a) Locations of study area, flux site, and sampling sites in Inner Mongolia, China. (b) Mean annual precipitation (P) across gradient of region from south and north, and (c) vs. elevation (blue solid line indicates smooth processing of x = 20) as retrieved from interpolated meteorological observations. Vegetation type was provided by Data Center for Resources and Environmental Sciences, Chinese Academy of Sciences (RESDC) (http://www.resdc.cn). (For interpretation of the references to colour in this figure legend, the reader is referred to the web version of this article.)

(NEE, g C $m^{-2}$ $d^{-1}$), and GPP (g C·$m^{-2}$·$d^{-1}$) between 2004 and 2005. Half-hourly measurements of ET (kg $H_2O$·$m^{-2}$·$d^{-1}$) were calculated using TA and LE (Donatelli et al., 2006), and half-hourly ET were summed to obtain daily amounts. Only original data (not gap-filled) were used in the process, and the dataset was quality-filtered according to the following rejection criterion: data under nocturnal low atmospheric turbulence conditions were excluded based on friction velocity ($u^*$) when $u^* < 0.20\ m\ s^{-1}$ (Han et al., 2014). Negative LE values were removed from the dataset.

### 2.4. Remote sensing data and its processing

To cover the absence of *in-situ* ET and GPP measurements across the study area, the remote sensing data were selected from the Moderate Resolution Imaging Spectroradiometer (MODIS, MOD16A2). We collected ET estimates with a spatial resolution of 500 m and 8-day temporal resolution, and GPP estimates from MOD17A2 with a spatial resolution of 1 km and 8-day temporal resolution data during the period of 2000–2016 (https://modis.gsfc.nasa.gov/data/). The tiles of MODIS products (h25v03, h25v04, h26v03, and h26v04) were mosaicked and redefined to an Albers projection. The 8-day summation of ET (kg·$m^{-2}$) and 8-day cumulative GPP (kg·C $m^{-2}$) estimates between 2004 and 2005 at the *in-situ* location were extracted, and then both the products were corrected against *in-situ* measurements at the daily scale (8-day intervals). To test the technique for partitioning ET using daily flux data in this study, ET and GPP estimates were averaged every 8 days. In addition, values at the administrative boundary vector data of the study area were obtained for the period of 2003–2012. Quality assessment (QA) of the performance of the two MODIS products was documented using *in-situ* measurements in the study area as shown later.

To conduct AGB estimates at a large spatial scale, the EVI time-series of satellite-based images (250 m spatial and 8-day temporal resolution, MOD09Q1) covering the period from 2003 to 2012 were obtained (https://modis.gsfc.nasa.gov/data/dataprod/mod09.php). Similar to ET and GPP estimates, EVI mosaic images were obtained, and geometric projection transformation was performed. The EVI estimates at the sampling locations and the administrative boundary vector for the study area were then extracted. To ensure the accuracy of EVI estimates, we set all invalid values to 0. Monthly EVI images were averaged from three 8-day EVIs in the current month, and the average EVI during the growing season was obtained using the maximum value composite (MVC) (Holben, 1986). The EVI was calculated follows (Eq. (1)):

$$EVI = G \times \frac{(\rho_{nir} - \rho_{red})}{\rho_{nir} + (C_1 \times \rho_{red} - C_2 \times \rho_{blue}) + L} \quad (1)$$

where, $\rho_{nir}$ represents the reflectance of the near-infrared band; $\rho_{blue}$ and $\rho_{red}$ represent the reflectance of the blue and red spectral bands, respectively; and G, $C_1$, $C_2$, and L are parameters set to 2.5, 6, 7.5 and 1, respectively. Then, based on the dataset, a statistical model was established for the inversion of AGB.

According to Wang et al. (2014), the fraction of T is directly linked to vegetation morphological attributes, in particular, leaf area index (LAI). Therefore, it is not surprising that LAI can act as a control over ET partitioning (Schlesinger and Jasechko 2014; Wang et al., 2014; Scott and Biederman, 2017). In this study, LAI products derived from MOD15A2 with a spatial resolution of 500 m and 8-day temporal resolution during the period 2000 to 2016 (https://modis.gsfc.nasa.gov/data) were obtained to evaluate the effect of vegetation cover on T/ET. The LAI data were processed similarly to ET and GPP data. The LAI values during the growing season each year were obtained by averaging all 8-day LAI values.

### 2.5. Standardized precipitation evapotranspiration index (SPEI)

Considerable research efforts have been devoted to quantifying drought, and different drought indices can result in different patterns of change during droughts, especially at small timescales (Burke, 2011). Drought events, defined using a multiscalar drought metric (i.e.,

**Table 1**
Categorization of drought/humid graded by the SPEI.

| Categories | SPEI values |
|---|---|
| Extreme drought | Less than −2.0 |
| Severe drought | (−2.0, −1.5] |
| Moderate drought | (−1.5, −1.0] |
| Mild drought | (−1.0, −0.5] |
| Near normal | (−0.5, 0.5] |
| Humid/Wet | More than 0.5 |

monthly, seasonally, half-yearly, and annual), can be well identified by the SPEI method based on a range of integration times (e.g., 12-month SPEI is integrated over the previous 12 months) (Vicente-Serrano et al., 2015; Beguería et al., 2014). Here, the main steps for calculating SPEI were as follows:

(1) Calculation of PET based on the P-M method.

Potential ET (PET) refers to the maximum E from the land surface when water supply is not limited under certain meteorological conditions (Allen and Ingram, 2002). The P-M method is used widely to estimate PET, e.g., grassland ecosystems (Zhang et al., 2016). Thus, PET was calculated as follows (Eq. (2)):

$$\mathrm{PET} = \frac{0.408\Delta(R_n - G) + \gamma\frac{900}{T_{mean}+273}U_2(VP_s - VP)}{\Delta + \gamma(1 + 0.34U_2)} \quad (2)$$

where, the unit of PET is mm/d; $R_n$ is net radiation at the surface; MJ/(m$^2$·d); G is soil heat flux, MJ/(m$^2$·d); $\gamma$ is the psychometric constant (kPa·°C$^{-1}$); Δ is the slope of saturated water vapor pressure, kPa·°C$^{-1}$; $U_2$ is wind speed at 2 m height, m·s$^{-1}$; $VP_s$ is mean saturated vapor pressure, kPa; VP is actual saturated vapor pressure, kPa; and $T_{mean}$ is mean temperature, °C. For detailed calculations, refer to relevant studies (Gong et al., 2006).

(2) Calculation of the difference ($D_i$) between monthly precipitation and PET, as follows (Eqs. (3) and (4)):

$$D_i = P_i - PET_i \quad (3)$$

$$D_n^k = \sum_{i=0}^{k-1}\left[\frac{2(i+1)}{k(k+1)}(P_{n-i} - PET_{n-i})\right], \ n \geqslant k \quad (4)$$

where, $D_i$ is the water deficit for the $i^{th}$ month (mm); $P_j$ is the $i^{th}$ month precipitation (mm); $PET_i$ is the $i^{th}$ month PET (mm); $D_n^k$is the accumulated $D_i$ at different time scales based on linearly decreasing weight; $k$ is time scale (month); and $n$ is the total calculated month.

(3) Use of the log-logistic probability distribution to fit the series of $D_i$, as follows (Eq. (5)):

$$f(x) = \frac{\beta}{\alpha}\left(\frac{x-\gamma}{\alpha}\right)^{\beta-1}\left[1 + \left(\left(\frac{x-\gamma}{\alpha}\right)^{\beta}\right)\right]^{-2} \quad (5)$$

where, x is $D_i$, and $\alpha$, $\beta$, and $\gamma$ are the scale, shape, and origin parameters, which were calculated by the L-moment method as follows (Eqs. (6)–(8)):

$$\beta = \frac{2w_1 - w_0}{6w_1 - w_0 - 6w_2} \quad (6)$$

$$\alpha = \frac{(w_0 - 2w_1)\beta}{\Gamma(1 + 1/\beta)\Gamma(1 - 1/\beta)} \quad (7)$$

$$\gamma = w_0 - \alpha\Gamma(1 + 1/\beta)\Gamma(1 - 1/\beta) \quad (8)$$

where, $\Gamma(\beta)$ is the gamma function of $\beta$. Thus, the cumulative density function of the $D_i$ probability density was calculated as showed below (Eq. (9)):

$$F(x) = \left[1 + \left(\frac{\alpha}{1-\gamma}\right)^{\beta}\right]^{-1} \quad (9)$$

(4) Standardization of the normal distribution of the $D_i$ series, and then obtain the corresponding SPEI (Eqs. (10) and (11)):

$$\mathrm{SPEI} = W - \frac{c_0 + c_1 w + c_2 w^2}{1 + d_1 w + d_2 w^2 + d_3 w^3}, \ P \leqslant 0.5, \ P = 1 - F(x) \quad (10)$$

$$\mathrm{SPEI} = -\frac{c_0 + c_1 w + c_2 w^2}{1 + d_1 w + d_2 w^2 + d_3 w^3}, \ P > 0.5, \ P = 1 - P \quad (11)$$

where, $W = \sqrt{-2\ln P}$, and the constants $c_0$, $c_1$, $c_2$, $d_1$, $d_2$, and $d_3$ are 2.51, 0.80, 0.01, 1.43, 0.19, and 0.001, respectively.

The SPEI values at the stations and across the study area were obtained using the interpolated daily meteorological data, and then the drought severity at different timescales was classified according to Table 1, where more negative values indicate more severe drought (Mckee et al., 1993; Vicente-Serrano et al., 2010). The SPEI at shorter timescales (i.e., 1-month, SPEI-1), represented as dry spell, reflects short-term and medium-term moisture conditions important for vegetation growth, whereas the SPEI at longer timescales (i.e., 12-month, SPEI-12) is probably related to streamflows and groundwater levels.

### 2.6. Approach for partitioning evapotranspiration

Employment of partitioning ET approach proposed by Zhou et al. (2014, 2016) is a critical part of our study. According to the essential differences between ET components, T provides a direct eco-hydrological link since it is coupled with $CO_2$ transfer (or $CO_2$ assimilation, A), which is related to stomatal conductance and atmospheric pressure. Based on the above concept, A and T were calculated as follows (Eqs. (12) and (13)):

$$A = g_s\frac{(c_a - c_i)}{p_a} \quad (12)$$

$$T = 1.6 \cdot g_s\frac{(e_i - e_a)}{p_a} \quad (13)$$

where, the units of A and T are $\mu mol \cdot m^{-2} \cdot s^{-1}$; $g_s$ is the stomatal conductance of $CO_2$, $\mu mol \cdot m^{-2} \cdot s^{-1}$; $p_a$ is the atmospheric pressure (hPa); $c_a - c_i$ and $e_i - e_a$ are the pressure difference between the inner leaf and ambient air for $CO_2$ and for water vapor (hPa), respectively.

According to the concept of uWUE ($uWUE = GPP \cdot VPD^{0.5}/ET$), this method considered the effect of VPD on water use efficiency. A linear relationship between T and VPD (hPa) was represented. At the leaf scale, water use efficiency, i.e., the ratio of A over T, was defined by VPD, thus the uWUE at the leaf scale ($uWUE_i$) was established considering the control of VPD on WUE. The $uWUE_i$ was calculated as follows (Eq. (14)):

$$uWUE_i = \frac{A\sqrt{VPD}}{T} \quad (14)$$

The VPD was assumed to be basically same within the uniform environment from the leaf level to the ecosystem level, and GPP was expressed as the accumulation of carbon assimilation. In this method, at the ecosystem level, potential uWUE ($uWUE_p$) is considered to be nearly identical to $uWUE_i$ when applying the coupled carbon-water relationship to all the leaves, and apparent uWUE ($uWUE_a$) is identical to observed uWUE affected by soil evaporation. The calculations of $uWUE_p$, $uWUE_a$, and the ratio of the two were as follows (Eqs. (15)–(17)):

$$uWUE_p = \frac{GPP\sqrt{VPD}}{T} \quad (15)$$

$$uWUE_a = \frac{GPP\sqrt{VPD}}{ET} \quad (16)$$

$$\frac{T}{ET} = \frac{uWUE_a}{uWUE_p} \quad (17)$$

Previous studies stated that T/ET follows a single-peak diurnal pattern and the diurnal peak value will reach unity when soil evaporation is negligible (Villegas et al., 2014; Wang and Yamanaka, 2014). Therefore, there is a critical assumption in the concept of uWUE, that is, when T is equal to ET (i.e., contribution of soil evaporation to ET is negligible) for a given uniform ecosystem, $uWUE_p$ is considered to be constant. In this study, two major analyses, including identification of field-based vegetation type and comparison of *in-situ* $uWUE_p$ and corrected $uWUE_p$ (calculations from corrected MODIS products using corresponding *in-situ* measurements), were used to test the constancy of $uWUE_p$ for all years across the study area.

### 2.7. Data analysis

All the dataset calculations and modelling were accomplished using Matlab (Matrix Laboratory, MathWorks), ArcGIS 10.2 Python (ArcGIS 10.2 with the Spatial Analyst extension and Python, ESRI), and R statistical software. Regression analyses were conducted and graphs were conducted using Origin 2017 (OriginLab, USA). Coefficient of determination ($R^2$), Spearman's correlation coefficients ($r$), root mean square error (RMSE), relative error (RE), and standard error ( ± sd) were calculated to assess the performance of corrected models (i.e., for correcting MODIS ET and GPP estimates) and the AGB inversion model. One-way ANOVA was used to test the difference among *in-situ* $uWUE_p$ measurements and corrected MODIS estimates. Statistical indicators and $p$-values were calculated to quantify the relationships and identify statistical differences among treatments. For all analyses, the confidence level of $p < 0.05$ was considered as statistically significant.

## 3. Results

### 3.1. Correction of satellite-based estimates

Prior to estimate the $uWUE_p$ and $uWUE_a$ values, *in-situ* ET and GPP observations were used to test the performance of MODIS estimates, even though some studies suggested that the estimates of satellite-based GPP and ET were able to capture the region-level seasonal variability in semiarid grassland of Inner Mongolia (Vetter et al., 2012). To keep the temporal resolution consistent, *in-situ* daily ET and GPP were integrated to values for 8-day intervals. Fig. 2(a) and (b) compared the two datasets (MODIS ET and GPP estimates, and *in-situ* ET and GPP measurements) at 8-day temporal scales during the 2004 and 2005 growing season. *In-situ* measurements were divided into two portions: one (training samples, values in 2004) for model establishment and the other (testing samples, values in 2005) for model verification. The results showed that MODIS ET underestimated the *in-situ* measurements by 13%. Similarly, MODIS GPP underestimated the *in situ* GPP measurements by up to 28.9%. To accurately evaluate ET components based on the concept of uWUE, it was necessary to correct the MODIS products. As illustrated in the inserts in Fig. 2(a) and (b), the corrected values of both ET and GPP were close to the observed values ($r$ of 0.97 and 0.98 respectively, and RMSE of 2.34 mm $8\,d^{-1}$ and 8.45 g C $m^{-2}$ $8\,d^{-1}$, respectively). After correction, the ET and GPP values tracked the dynamics of the corresponding measurements well. These results indicated that corrected MODIS ET and GPP were accurate and preferable as parameters for developing the ET partitioning model in this study.

### 3.2. Grassland aboveground biomass (AGB) inversion

Based on previous research on AGB inversion for grassland ecosystems, we selected a linear regression between EVI and AGB to estimate grassland AGB (Todd et al., 1998; Li et al., 2007). Here, sampling dataset comprised 130 quadrats of 1 m × 1 m and was divided into two portions: one (55 samples in 2016) for model correction and the other (75 samples in 2015) for model verification. The performance of the inversion model between EVI and AGB was evaluated using several statistical indexes, e.g., $R^2$, RMSE, and RE. The inversion model was as follows (Eq. (16)):

$$AGB_i = \alpha \times EVI_i + \beta \quad (16)$$

This inversion model was used to characterize the variations in grassland AGB during the growing season. As shown in Fig. 3, there was a strong positive correlation between AGB and EVI at the site scale ($R^2 = 0.65$, $p < 0.01$). To avoid over-fitting, we then verified the validity of the model for estimating grassland AGB by calculating $R^2$, the RMSE and RE using the validation dataset. We detected a strong relationship between the AGB estimated from the model and measured AGB at the site scale ($R^2 = 0.93$, $p < 0.01$, RMSE = 37.4 g/$m^2$, RE = 13.7%) (Fig. 3). Thus, the EVI-based AGB inversion model showed good performance for estimating grassland AGB in this study area, representing the ability of EVI to estimate AGB across the study area.

### 3.3. Seasonal variations of droughts across the study area

The sensitivity of the SPEI value differed on different time scales. Based on the SPEI drought index categories, values lower than −0.5 indicate a drought event across the study area, whereas those higher than 0.5 indicate a humid/wet climate. The fluctuation of wetness and dryness was more significant at the shorted timescales (e.g., 1-month, Fig. S1) than at longer timescales (e.g., 12-month, Fig. 4a). Additionally, there was a significant decrease ($p < 0.01$) in the inter-annual variation of SPEI values during the period of 1961–2015. This indicated that there were increases in the frequency and severity of droughts after 2000 (Fig. 4a), as reported previously by Qu (2015) and the National Oceanic and Atmosphere Administration (NOAA, 2012). Consecutive drought events (SPEI < −1.0) occurred across the study area during the period of 2004–2011, with an exception of 2008. It was noted that extreme droughts occurred in 2007. During the prolonged drought period of 2004–2011, dry spells were more frequent and severe during the growing season than during the non-growing season, especially in 2005, 2007, and 2009 (Fig. 4b). There has been a combination of increased aridity and prolonged droughts at the 12-month timescale since 2000, and more frequent dry spells during the growing season were the main contributors to the prolonged yearly drought from 2004 to 2011.

Hence, in this study, we selected the period of 2003–2012 as the study period (i.e., pre-, during, and post-drought) to analyze the effects of prolonged drought on ET components (i.e., T/ET in this study), and on vegetation productivity in water-limited grasslands.

### 3.4. Ecosystem-level potential uWUE estimation

In this study, the flux site was established in a relatively homogeneous ecosystem, where there is minimal spatial variation in the structural characteristics of the vegetation. Considering the field-based results of vegetation type (Table S1, Supplementary Material) and the relationships between geography and climate (Fig. 1b and c), this study area was considered to be a uniform ecosystem. Thus, $uWUE_p$ calculated from the flux data was reasonable and valid to apply for the whole grassland ecosystem. To further test the assumption that $uWUE_p$ was essentially constant across the study years, the average $uWUE_p$ for the study period was compared with the average $uWUE_p$ values for site-year. As shown in Fig. 5, $uWUE_p$ was estimated as the regression slope for the 95th quantile regression (i.e., upper bound between $GPP{\cdot}VPD^{0.5}$ and ET) with all the daily ET and GPP data during the growing season in 2004 and 2005 for the flux site, and the corresponding daily VPD. The results showed that the slope of the 95th quantile regression line,

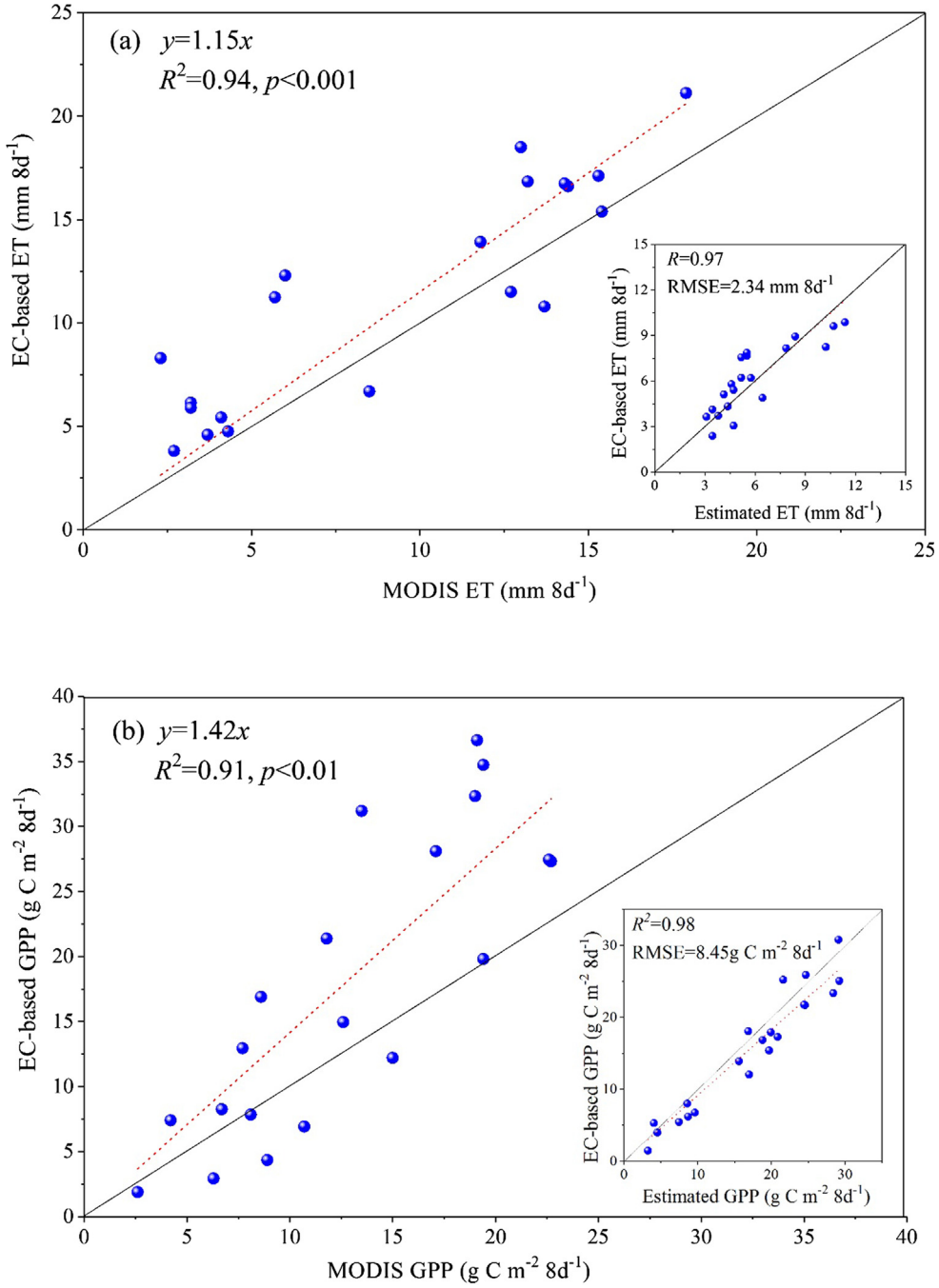


**Fig. 2.** Comparisons and validation results of MODIS 8-day ET estimates (a) and GPP estimates (b) against *in-situ* ET and GPP measurements. Inserts illustrate good performance of two correction models, i.e., $ET_{EC} = 1.15 \times ET_{MOD}$, and $GPP_{EC} = 1.42 \times GPP_{MOD}$. Data in 2004 and 2005 were used for correction and validation, respectively. Red dashed lines represent linear regression lines. Black solid line = 1:1 line. (For interpretation of the references to colour in this figure legend, the reader is referred to the web version of this article.)

i.e., the $uWUE_p$, was 14.7 g C·hPa$^{0.5}$/kg $H_2O$ for the flux site.

This study also calculated the $uWUE_p$ using *in-situ* 8-day interval measurements (i.e., $EC_{8d}$ $uWUE_p$) matching with the temporal resolution of the MODIS estimates. The $uWUE_p$ using corrected MODIS estimates (hereafter, $cMOD_{8d}$) was calculated for the periods of 2004–2005 and 2003–2012, respectively. The insert in Fig. 6 showed the comparison between the measured $uWUE_p$ (i.e., $EC_d$ and $EC_{8d}$) and the estimated (i.e., $cMOD_{8d}$) values for the periods of 2004–2005 and 2003–2012. As shown in the figure, there was no significant difference between them ($p > 0.05$). More specifically, in 2004 and 2005, $EC_d$ $uWUE_p$ was higher than $EC_{8d}$ with an error of 11%. The $EC_{8d}$ $uWUE_p$ values were higher than $cMOD_{8d}$ values for the periods of 2004–2005 and 2003–2012, with errors of 0.06% and 0.01%, respectively. Additionally, we compared annual and long-term (2003–2012) average $uWUE_p$ across the study area using corrected MODIS estimates. The results showed that the departures of annual $uWUE_p$ values from the mean was within 0–10%, except in 2012 (10.1%). Since there was little difference between the estimated annual $uWUE_p$ and the mean value, we concluded that $uWUE_p$ was relatively consistent. This confirmed that it was reasonable to assume that the long-term $uWUE_p$ was essentially constant across the study period.

The $uWUE_p$ for the study area was higher than those listed in the Ameriflux network (http://public.ornl.gov/ameriflux), which were estimated in previous studies for the same vegetation type (i.e.,

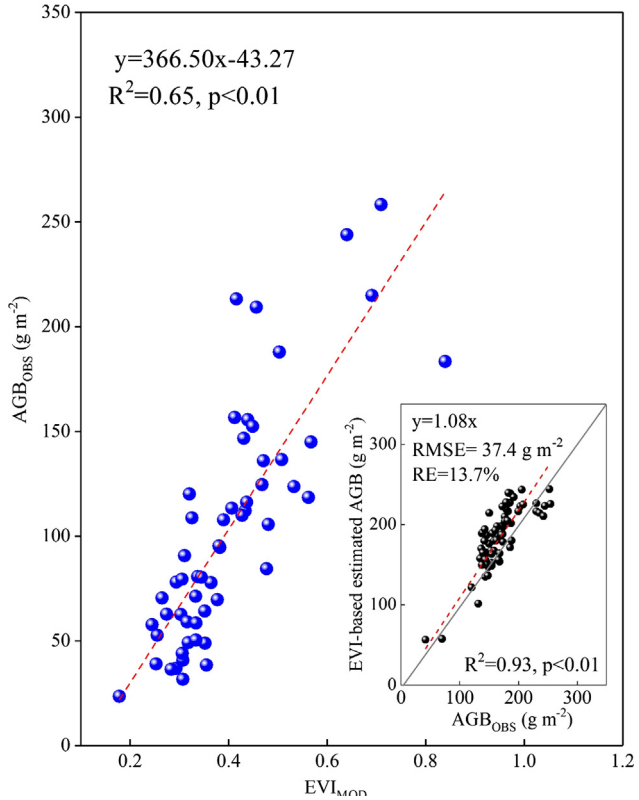


**Fig. 3.** *In-situ* relationship between measured AGB ($AGB_{OBS}$) and MODIS EVI ($EVI_{MOD}$) for 55 sites. Red dashed lines represent linear regression applied to estimate AGB (AGB = 366.5 × EVI-43.27). Insert shows the fitted regression between EVI-based estimated AGB and $AGB_{OBS}$ for 75 sites. The grey line in insert shows 1:1 line. (For interpretation of the references to colour in this figure legend, the reader is referred to the web version of this article.)

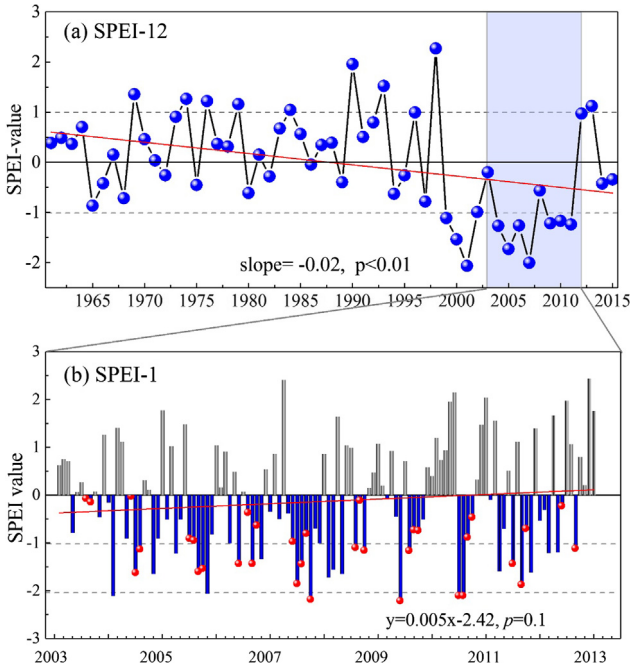


**Fig. 4.** Time series of SPEI at 12-month scale for the period of 1961–2015 (a) and at 1-month scale during study period of 2003–2012 (pre-, during and post-drought period) (b) across study area. More negative values indicate more severe drought. Red circles indicate drought spells during growing season. Red solid line represents linear regression line. (For interpretation of the references to colour in this figure legend, the reader is referred to the web version of this article.)

grassland); for example, 13.83 g C·$hPa^{0.5}$/kg $H_2O$ for the US-Var site in 2001–2007 (Xu and Baldocchi, 2004), and 12.99 g C·$hPa^{0.5}$/kg $H_2O$ for the US-Wlr site between 2002 and 2004 (Coulter et al., 2006; Wilson and Meyers, 2007). Those two sites experienced a humid climate with average annual precipitation of more than 500 mm and mean temperature higher than 13 °C (more details are shown in Supplementary Table S2). Previous studies suggested that $uWUE_p$ increases as the water supply changes from wet to dry (e.g., wetlands, lowlands, dryland, and sand) (Poncecampos et al., 2013). Morecroft and Woodward (1990) also found that the higher the humidity, the lower the $uWUE_p$, which supported our findings that the $uWUE_p$ was higher than for the other two US grasslands mentioned above. Moreover, the $uWUE_p$ was higher under medium water stress than under severe water stress for vegetation. Therefore, $uWUE_p$ was estimated to be higher for the NMG site than for the other two sites mainly because of the climatic differences between the NMG (semiarid region) and the US-Var and US-Wlr sites (humid climate region).

### 3.5. Variations in apparent uWUE and T/ET to prolonged drought

The variation in $uWUE_a$ estimated as the linear regression slope using daily data (8-day intervals) for ET, GPP, and VPD, was shown in Fig. 7. The results indicated that the linear regression slopes (i.e., $uWUE_a$ values) varied under altered hydroclimatic conditions with values of 7.59 g C·$hPa^{0.5}$/kg $H_2O$ in 2003 (Fig. 7a, pre-drought), 6.50 ± 0.44 g C·$hPa^{0.5}$/kg $H_2O$ during the drought period of 2004–2011 (Fig. 7b–i), and 7.93 g C·$hPa^{0.5}$/kg $H_2O$ in 2012 (Fig. 7j, post-drought). There was a decrease in $uWUE_a$ when drought initially occurred across the study area following a normal year (Fig. 7a and b). During the prolonged drought period, there was no significant variation

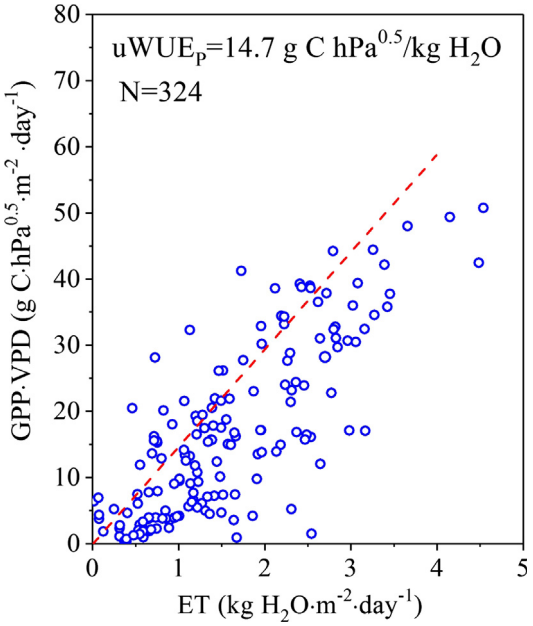


**Fig. 5.** The 95th quantile regression using all daily data for the flux site during growing season between 2004 and 2005 (measured GPP during DOY 122–284 in 2004 and during DOY 121–283 in 2005). Daily ET and GPP data were obtained by integrating half-hourly values from flux site, and daily vapor pressure deficit (VPD) data were obtained from meteorological data from China Meteorological Data Service Center (CMDC, http://data.cma.cn/site/index.html). The intercept was set to zero for quantile regression.

in $uWUE_a$, with an exception of 2007–2008 (Fig. 7b–i). These results illustrated that increases in the frequency and duration of drought did not necessarily lead to significant changes in ecosystem $uWUE_a$, but the

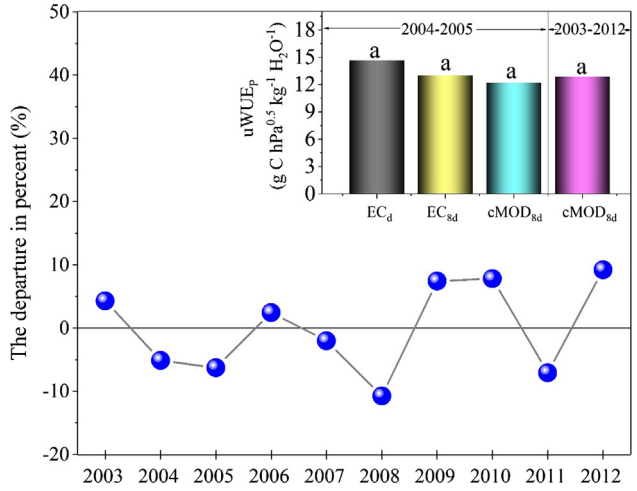


**Fig. 6.** Departures of uWUE$_p$ estimated by corrected MODIS data in each year from long term average (i.e., 2003–2012). Insert shows differences in mean uWUE$_p$ using daily *in-situ* values (EC$_d$), 8-day interval *in-situ* values (EC$_{8d}$), and corrected MODIS estimates (cMOD$_{8d}$) in 2004 and 2005, and cMOD$_{8d}$ in 2003–2012 for the flux site. Columns labelled with the same letter are not significantly different (one-way ANOVA, $P > 0.05$).

increasing severity of drought, especially extreme drought following a continuing drought, reduced uWUE$_a$ (Fig. 7e and f). In the humid/wet year following prolonged drought, high precipitation increased the ecosystem uWUE$_a$, resulting from replenishment of soil water available for vegetation growth (Fig. 7j).

The corresponding annual T/ET ratios were in the range of 0.46–0.62. The estimated annual T/ET during the period of 2003–2012 was 0.53 ± 0.05 (0.59 in the pre-drought year, 0.51 ± 0.03 during the prolonged drought period, and 0.62 in the post-drought year). The T/ET ratio decreased when moderate drought occurred across the study area, indicating that soil evaporation was the main contributor to the increase in ET. As the drought was more severe and persistent, the T/ET basically remained constant, then fell to its minimum value during and following the extreme drought. The T/ET ratio returned to normal or even higher levels during the increase in water availability after the prolonged drought. The estimated annual T/ET ratio (0.53 ± 0.05) during the study period was slightly lower than those reported by Zhou et al. (2016; T/ET ratio of 0.56 ± 0.05) and Schlesinger and Jasechko (2014; T/ET ratio of 0.57 ± 0.19).

## 4. Discussion

### 4.1. Contributions of precipitation and temperature to drought

To identify the contributions of precipitation and temperature to prolonged drought, we analyzed interannual variations in annual precipitation and mean temperature over the past 50 years, as shown in Fig. 8. Increases in precipitation deficits and mean temperature immediately led to increases in the frequency, magnitude, and duration of droughts. The anomalies in precipitation and temperature indicated that alternation of water deficit and water surplus was frequent in the study area, and that the study area has experienced continuous

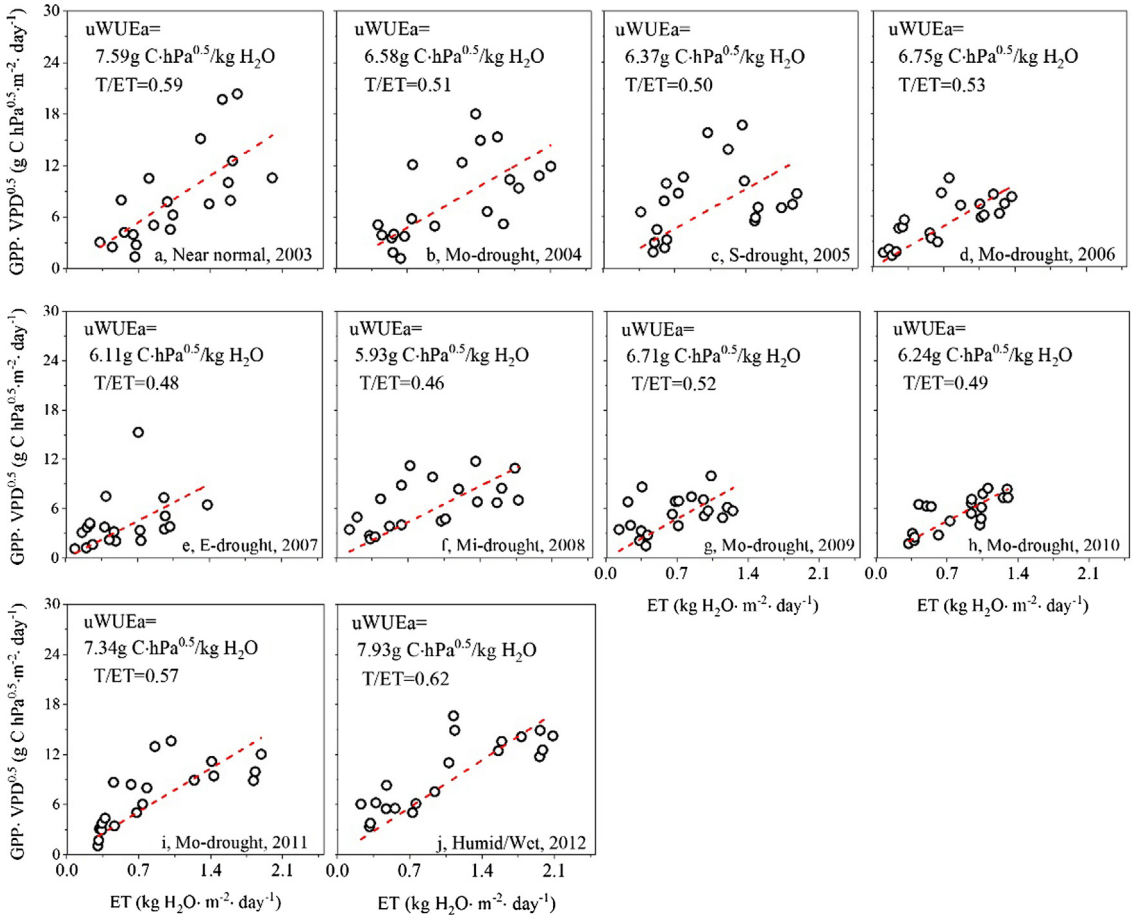


**Fig. 7.** Linear regression using daily corrected ET and GPP estimates and daily VPD data (8-day interval) during the growing season from 2003 to 2012. Pre-drought year, 2003; drought period, 2004–2011; post- drought, 2012; (a–j). Mi-drought, mild drought; Mo-drought, moderate drought; S-drought, severe drought; E-drought, extreme drought. Each sub-graph contains 20 points (N = 20). The intercept was set to zero for linear regressions.

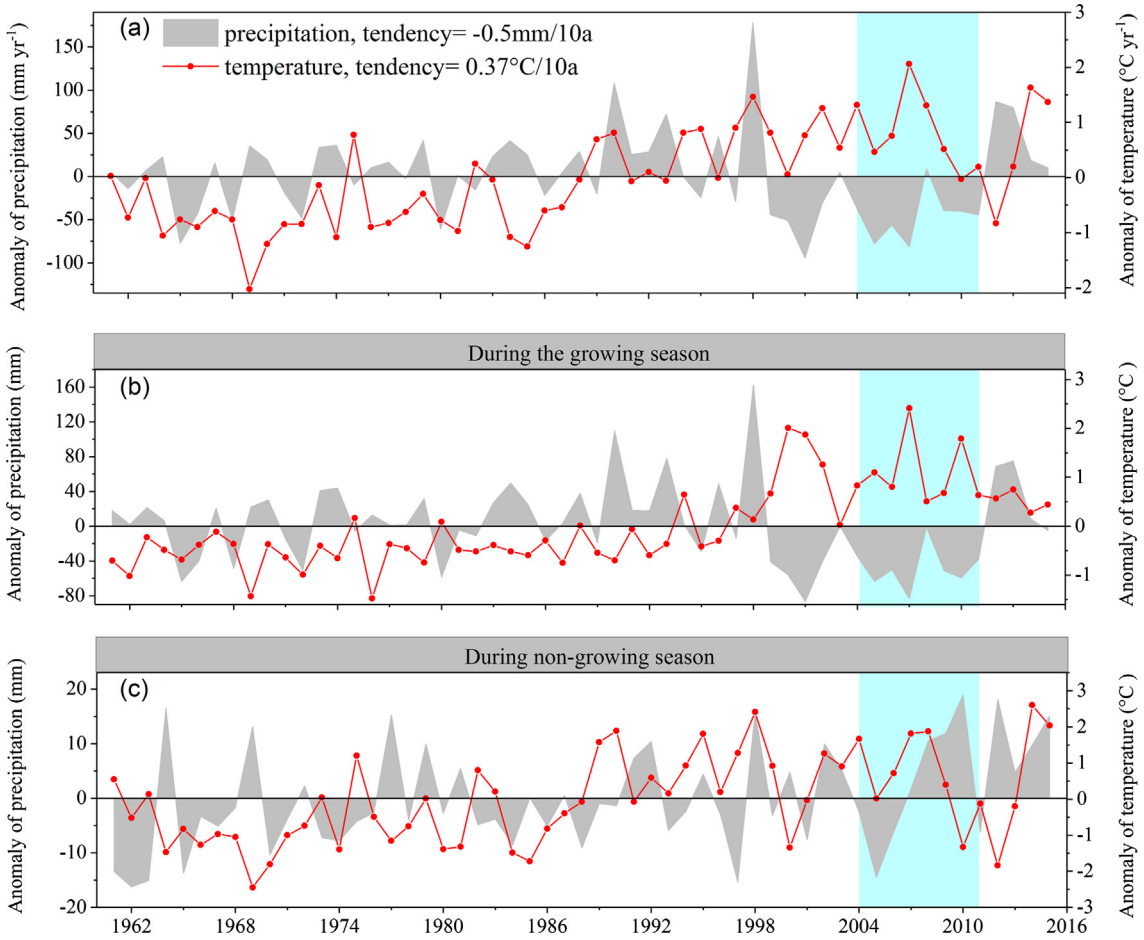


**Fig. 8.** Anomalies in annual precipitation and mean annual temperature (a), precipitation and temperature during the growing season (b), and during the non-growing season (c) across study area over last 50 years. Shaded area indicates drought period.

warming since the 2000s. Hence, increases in the duration and severity of droughts since the 2000s resulted from the joint actions of increasing air temperature and decreasing precipitation. The mean annual precipitation of 246 ± 28 mm $yr^{-1}$ during 2004–2011 (prolonged drought) was significantly lower than that during 1990–1997 (average precipitation conditions, 320 ± 47 mm $yr^{-1}$). It was also lower than the long-term (50-yr) average precipitation of 292 ± 50 mm $yr^{-1}$. The mean temperature was different significantly among decades, warming from 0.90 ± 0.57 °C in 1961–1980 to 1.97 ± 0.80 °C in 1981–2015. The mean temperature of 2.41 ± 0.69 °C during the prolonged drought period was higher than that of 1.58 ± 0.89 °C over the last 50 years, indicating that more regions experienced warming close to 1 °C.

The variation in precipitation during the growing season explained 86.7 ± 0.03% of annual precipitation in the last 50 years (Fig. 8b and c). Precipitation during the growing season showed patterns of increases to decreases after the 1980s, which differed from patterns during the non-growing season. During the non-growing season, the variation in mean temperature was in good agreement with average annual change, indicating that temperature variation in the non-growing season controlled annual mean temperature. Furthermore, the mean temperatures increased significantly both in the growing season and the non-growing season, especially after 2000 ($p < 0.05$). Overall, the study area experienced consecutive droughts from 2004 to 2011 because of prolonged higher temperatures and less precipitation since 2000, although the highest mean precipitation in the non-growing season appeared in 2008–2010.

### 4.2. Changing responses of AGB and ET partitioning to prolonged drought

The climatic and surface controls of T/ET add complexity to the description of patterns of T/ET (Schlesinger and Jasechko, 2014; Wang et al., 2014). Scanlon and Kustas (2012) reported that vegetation was a first-order factor affecting ET partitioning. The LAI, as a key proxy of vegetation morphology, was found to be positively related to T (Good et al., 2014; Schlesinger and Jasechko, 2014). We detected correlations between the annual T/ET ratios and precipitation, temperature, LAI, and estimated AGB (Fig. 9a–d). The T/ET ratio was most strongly correlated with AGB ($R^2 = 0.80$, $p = 1.0$), followed by LAI ($R^2 = 0.58$, $p < 0.01$) across the study area during the growing season. The correlation coefficient was relatively low for the relationship between T/ET ratio and precipitation ($R^2 = 0.49$, $p < 0.05$), and the lowest for the relationship between the T/ET ratio and air temperature ($R^2 = 0.31$, $p = 0.1$). The significant positive correlation between precipitation and T/ET indicated that precipitation controlled increases in LAI and T/ET mainly via its effect to supply soil relative humidity (RD) (Wang et al., 2014). We also found that the T/ET became larger as the AGB and LAI increased. Therefore, AGB (or EVI), LAI, as well as some climatic variables (precipitation, or RD) were most likely to reflect the variation in T/ET across the study area during the prolonged drought period.

To further explore the response of ET partitioning to prolonged drought, we plotted the interannual variations in AGB, ET, and the annual T/ET ratio under altered hydroclimatic conditions (Fig. 10). The average T/ET ratio was lower during the study period of 2003–2012 (0.55 ± 0.06) than in the pre-drought (0.65) and post-drought years (0.72). Vegetation growth (i.e., AGB) was also responsive to altered hydroclimatic conditions. According to the variations in AGB, this study

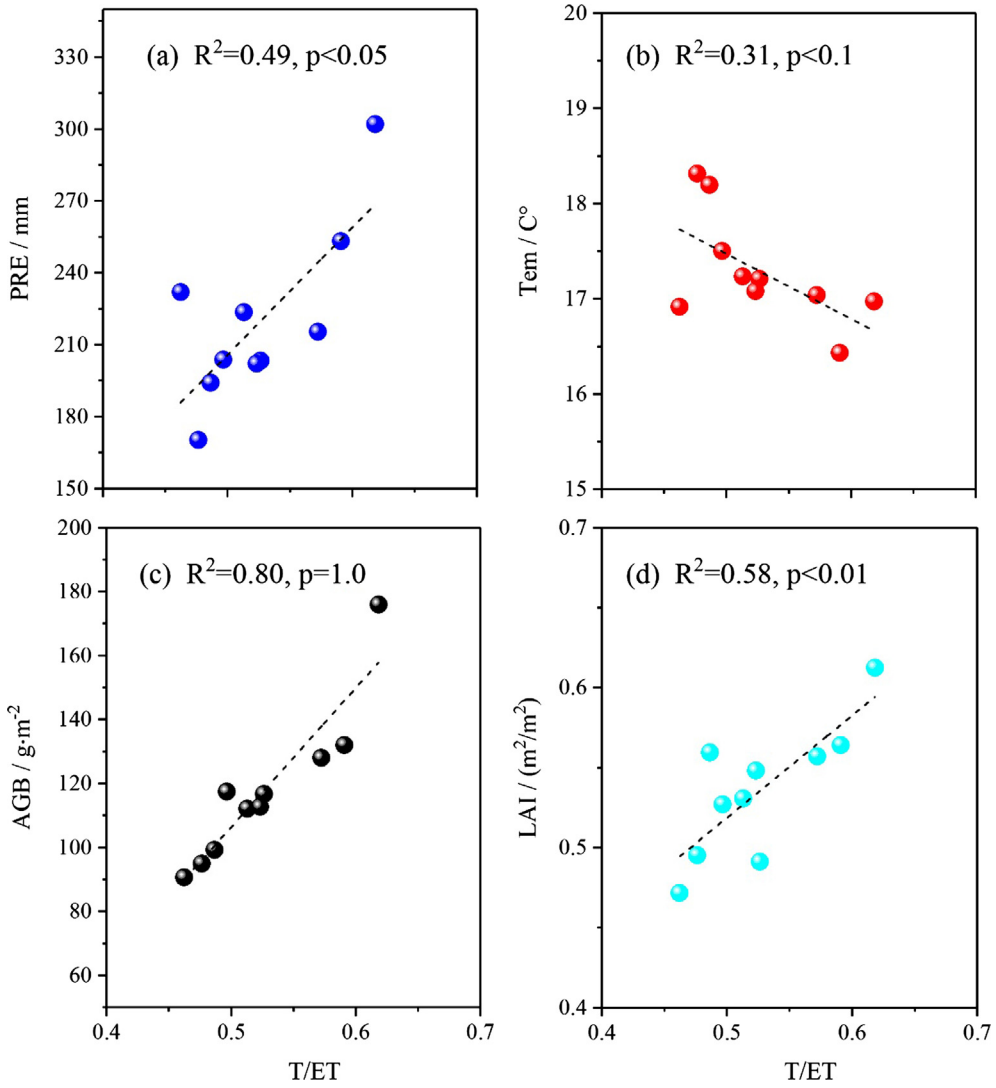


**Fig. 9.** Correlations between T/ET and precipitation, temperature, LAI, and AGB across study area during the growing season in study period (i.e., 2003–2012). Regression lines are shown. Number of solid circles in each sub-graph is 10 (i.e., N = 10).

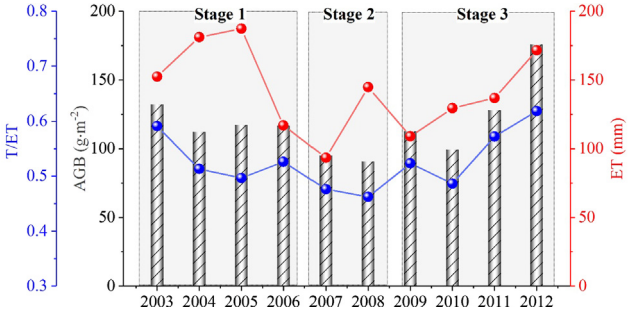


**Fig. 10.** Interannual variations in T/ET ratio, corrected ET, and EVI-estimated AGB during the growing season across study area. Gray areas indicate three different response stages of ecosystem functioning to drought according to varying characteristics of vegetation growth: ecosystem maintenance (stage 1), ecosystem degradation (stage 2), and ecosystem recovery (stage 3).

divided the study period (2003–2012) into three stages, ecosystem maintenance (stage 1), ecosystem degradation (stage 2), and ecosystem recovery (stage 3), to further examine the response of vegetation growth to drought stress in different climates. In the first stage, the AGB decreased from its pre-drought value when moderate drought hit across the study area. This revealed that the vegetation rapidly responded to changing water availability and that the ecosystem was sensitive to hydroclimatic disturbance (Vicente-Serrano et al., 2013). The T would decrease since the water use efficiency increased to sustain productivity in that year. Thus, the corresponding T/ET ratio decreased mainly owing to an increase in ET, which might imply an increase in soil evaporation. With the persistent drought between 2005 and 2006, the variation in AGB was only slightly linked to drought intensity, indicating weak sensitivity of vegetation to consecutive drought. Continuous water loss contributed to the slight increase in the T/ET ratio, indicating that soil evaporation loss was greater than that from plant transpiration. Additionally, this result might be explained by the fact that the ecosystem could sustain vegetation growth by decreasing T (i.e., increasing WUE), as reflected by the sharp decrease in ET from 2005 to 2006 (Poncecampos et al., 2013). On the basis of these results, we concluded that at the first stage, grassland ecosystem exhibited an ability to recover from disturbances and sustain productivity through self-regulation to a certain extent.

In the second stage, both AGB and the T/ET ratio decreased when extreme drought occurred in 2007. That is, the vegetation decreased in the study area under extreme drought. Knapp and Smith (2001) reported that extreme drought resulted in plant dieback and mortality. On the basis of the climatic conditions in 2007 (Fig. 9), we suggested that this degradation was mainly caused by continuous water stress with the

least precipitation and highest temperatures. Although precipitation was higher during the non-growing season in 2008 than in the previous years, the ecosystem continued to show the lowest AGB levels without recovery. Thus, the extreme drought at this stage decreased grassland productivity, potentially resulting in vegetation mortality (Knapp and Smith, 2001) and the break-down of its self-regulating capacity (He et al., 2018). Changes in the self-regulating capacity of the ecosystem might result from a shift in species composition, like that reported Poncecampos et al. (2013).

During the third stage from 2009 to 2012, the increase in precipitation during the non-growing season alleviated water stress for vegetation growth (Fig. 8c). Both the AGB and ET increased, indicating that more moisture was available for vegetation to support plant transpiration and soil evaporation. The increases in the AGB and ET were accompanied by a corresponding increase in T/ET, indicating vegetation had resumed growing by 2012 (Poncecampos et al., 2013). In the humid year of 2012 following consecutive drought, precipitation pulses vastly alleviated water deficits and increased soil water storage availability for ecosystem recovery. Thus, the AGB, T/ET ratio and ET increased to reach their maximum values in the third stage. These results revealed the different responses of grassland ecosystems to altered hydroclimatic conditions by exploring the variation in T/ET to prolonged drought. Extreme drought during prolonged droughts would likely degenerate the ecosystem, showing an obvious reduction in vegetation productivity. Thus, our results indicated that the semiarid grassland ecosystem was sensitive to drought stress, and had an ability to rapid recover with an increase in water availability.

### 4.3. Uncertainty and limitations

In this study, we examined the responses of ET components to prolonged drought for grassland ecosystem based on the uWUE method. However, there are some limitations and uncertainties. First, the uncertainties derived from *in-situ* ET and GPP measurements were not considered, although they are commonly used as a benchmark to validate satellite-based corresponding products (Yu et al., 2006; Lin, 2015). Natural vegetation often is less than homogeneous both vertically and horizontally, so the vegetation characteristics in a flux site may not be representative of the vegetation of interest, especially for a large region (Rana and Katerji, 2000). Additionally, the limited source area of the flux site mismatched with the satellite-based pixels (500 and 1000 m). These factors resulted in uncertainties in the validation of satellite-based products to a certain extent. Another important constraint stemmed from field-sampled biomass. We have not considered the differences in these species in the sampling survey, but assumed that all had an equal importance. Thus, the AGB may have been overestimated by the inversion model related to the EVI.

Second, we found some degree of uncertainty in the corrected MODIS GPP and ET estimates, even though the satellite-based estimates corrected against the corresponding measurements at the *in-situ* level provided acceptable accuracy (Fig. 2). In this study, after corrections for MODIS ET and GPP estimates, corrected ET values were approximately identical to measured values, whereas the corrected GPP estimates still underestimated by 8.7%. Consequently, both $uWUE_p$ and $uWUE_a$ were underestimated by 8.7% according to the Eqs. (15) and (16).

Third, in our analyses, we assumed a constant $uWUE_p$ across all years in the study area (Zhou et al., 2016). However, the $uWUE_p$ may be expected to change dramatically due to the extreme drought and/or vegetation changes (Zhou et al., 2014, 2016). Thus, we tested this assumption by analyzing the difference between $uWUE_p$ in each year and its long-term average (Fig. 6), and found that there were certain discrepancies in the annual $uWUE_p$ during 2003–2012. The greatest departures of $uWUE_p$ values from the average were around 10% in a humid and following an extreme drought year (Fig. 6). According to Zhou et al. (2016), this relative small variation in $uWUE_p$ may not induce large uncertainties in ET partitioning and therefore the uWUE method to estimate ET partitioning could be used in our research area. On the other hand, additional data for more years are necessary to explore the possible changes in $uWUE_p$ considering the expected drought in future.

In most of the published studies, there were significant uncertainties around the contribution of T to ET (i.e., T/ET) reflected by the wide range of T/ET values (Good et al., 2015; Maxwell and Condon. 2016). To quantitatively evaluate the difference resulting from the T/ET, we compared the T/ET values in this study with those reported in the literature. The assumption that T will be equal to ET during the growing season with high vegetation cover may be imprecise, because vegetation is relatively sparse and soil evaporation cannot be ignored in the study area. Consequently, the $uWUE_p$ may be underestimated and T/ET overestimated.

## 5. Conclusion

We explored the responses of ET partitioning to prolonged droughts based on EC measurements and MODIS estimates using the uWUE method proposed by Zhou et al. (2014, 2016), and identified the factors controlling T/ET. Prolonged drought during 2004–2011 substantially restricted vegetation growth and reduced grassland productivity, further changed the contributions of the two components to ET. The T/ET ratio was well represented by AGB, LAI, and precipitation under long-lasting and warming drought conditions. The response of T/ET also indicated that the ecosystem was able to resist the drought disturbance and retain vegetation growth during the initial period of drought. When extreme drought hit, the decrease in T/ET demonstrated that the ecosystem was unable to sustain productivity due to an obvious reduction in water availability. In the humid years following prolonged drought, an increase in the T/ET ratio represented recovery of the ecosystem. Our results highlight the need to understand the major flux processes (i.e., E, T, and ET) under prolonged drought conditions and the factors controlling ET in a semiarid grassland. These findings will improve our understanding of the specific responses of the grassland ecosystem to prolonged droughts.

## Acknowledgements

This study was supported by the National Natural Science Foundation of China (Grant No. 51679006, Grant No. 51620105003 and Grant No. 51779007), the Evaluation of Resources–Environmental Carrying Capacity in Typical Ecological Zones of Xinganling (Grant No. 12120115051201).

## Appendix A. Supplementary data

Supplementary data associated with this article can be found, in the online version, at https://doi.org/10.1016/j.jhydrol.2018.06.048.

## References

Allen, M.R., Ingram, W.J., 2002. Constraints on future changes in climate and the hydrologic cycle. Nature 419, 224.
Beguería, S., Vicente Serrano, S.M., Reig, F., Latorre, B., 2014. Standardized precipitation evapotranspiration index (SPEI) revisited: parameter fitting, evapotranspiration models, tools, datasets and drought monitoring. Int. J. Climatol. 34, 3001–3023.
Berkelhammer, M., Noone, D.C., Wong, T.E., Burns, S.P., Knowles, J.F., Kaushik, A., Blanken, P.D., Williams, M.W., 2016. Convergent approaches to determine an ecosystem's transpiration fraction. Global Biogeochem. Cycles 30.
Burke, E.J., 2011. Understanding the sensitivity of different drought metrics to the drivers of drought under increased atmospheric $CO_2$. J. Hydrometeorol. 12, 1378–1394.
Coners, H., Babel, W., Willinghöfer, S., Biermann, T., Köhler, L., Seeber, E., Foken, T., Ma, Y., Yang, Y., Miehe, G., 2016. Evapotranspiration and water balance of high-elevation grassland on the Tibetan Plateau. J. Hydrol. 533, 557–566.
Coulter, R.L., Pekour, M.S., Cook, D.R., Klazura, G.E., Martin, T.J., Lucas, J.D., 2006. Surface energy and carbon dioxide fluxes above different vegetation types within ABLE. Agric. For. Meteorol. 136, 147–158.

Coyle, D.R.C.R., Coleman, M.D., Aubrey, D.P.A.P., 2008. Above- and below-ground biomass accumulation, production, and distribution of sweetgum and loblolly pine grown with irrigation and fertilization. Can. J. For. Res. 38, 1335–1348.
Dai, A., 2011a. Drought under global warming: a review. Clim. Change 2, 45–65.
Dai, A., 2011b. Characteristics and trends in various forms of the Palmer Drought Severity Index during 1900–2008. J. Geophys. Res. Atmos. 116, 1248–1256.
Donatelli, M., Bellocchi, G., Carlini, L., 2006. Sharing knowledge via software components: models on reference evapotran-spiration. Eur. J. Agron. 24, 186–192.
Fisher, J.B., Tu, K.P., Baldocchi, D.D., 2008. Global estimates of the land–atmosphere water flux based on monthly AVHRR and ISLSCP-II data, validated at 16 FluxNet sites. Remote Sens. Environ. 112, 901–919.
Gong, L., Xu, C.Y., Chen, D., Halldin, S., Chen, Y.D., 2006. Sensitivity of the Penman-Monteith reference evapotranspiration to key climatic variables in the Changjiang (Yangtze River) basin. J. Hydrol. 329, 620–629.
Good, S.P., Soderberg, K., Guan, K., King, E.G., Scanlon, T.M., Caylor, K.K., 2014. $\delta^2$H isotopic flux partitioning of evapotranspiration over a grass field following a water pulse and subsequent dry down. Water Resour.Res. 50, 1410–1432.
Good, S.P., Noone, D., Bowen, G., 2015. Water resources. Hydrologic connectivity constrains partitioning of global terrestrial water fluxes. Science 349, 175–177.
Hall, D.O., Scurlock, J.M.O., Ojima, D.S., Parton, W.J., 2000. The Carbon Cycle: Grasslands and the Global Carbon Cycle: Modeling the Effects of Climate Change. Cambridge University Press.
Han, D., Wang, G., Xue, B., Liu, T., Yinglan, A., Xu, X., 2018. Evaluation of semiarid grassland degradation in north china from multiple perspectives. Ecol. Eng. 112, 41–50.
Han, G., Xing, Q., Yu, J., Luo, Y., Li, D., Yang, L., Wang, G., Mao, P., Xie, B., Mikle, N., 2014. Agricultural reclamation effects on ecosystem $CO_2$ exchange of a coastal wetland in the Yellow River Delta. Agric. Ecosyst. Environ. 196, 187–198.
He, B., Huang, L., Chen, Z., Wang, H., 2018. Weakening sensitivity of global vegetation to long-term droughts. Sci. China Earth Sci. 1, 1–11.
Holben, B.N., 1986. Characteristics of maximum-value composite images from temporal AVHRR data. Int. J. Remote Sens. 7, 1417–1434.
Huete, A., Didan, K., Miura, T., Rodriguez, E.P., Gao, X., Ferreira, L.G., 2002. Overview of the radiometric and biophysical performance of the MODIS vegetation indices. Remote Sens. Environ. 83, 195–213.
Knapp, A.K., Smith, M.D., 2001. Variation among biomes in temporal dynamics of aboveground primary production. Science 291, 481.
Kurtzman, D., Navon, S., Morin, E., 2009. Improving interpolation of daily precipitation for hydrologic modelling: spatial patterns of preferred interpolators. Hydrol. Process. 23, 3281–3291.
Lawrence, D.M., Thornton, P.E., Oleson, K.W., Bonan, G.B., 2007. The partitioning of evapotranspiration into transpiration, soil evaporation, and canopy evaporation in a GCM: impacts on land atmosphere interaction. J. Hydrometeorol. 8, 862.
Leuning, R., Zhang, Y.Q., Rajaud, A., Cleugh, H., Tu, K., 2008. A simple surface conductance model to estimate regional evaporation using MODIS leaf area index and the Penman-Monteith equation. Water Resour. Res. 44, 652–655.
Li, S.G., Asanuma, J., Kotani, A., Davaa, G., Oyunbaatar, D., 2007. Evapotranspiration from a Mongolian steppe under grazing and its environmental constraints. J. Hydrol. 333, 133–143.
Lin, Z., 2015. Trends in land surface evapotranspiration across China with remotely sensed NDVI and climatological data for 1981–2010. Int. Assoc. Sci. Hydrol. Bull. 60, 2163–2177.
Maxwell, R.M., Condon, L.E., 2016. Connections between groundwater flow and transpiration partitioning. Science 353, 377.
Mckee T.B., Doesken N.J., Kleist J., 1993. The relationship of drought frequency and duration to time scales. In: 8th Conference on applied climatology, 17–22 Jan, Anaheim, 179–184.
Méndez-Barroso, L.A., Vivoni, E.R., Watts, C.J., Rodríguez, J.C., 2009. Seasonal and interannual relations between precipitation, surface soil moisture and vegetation dynamics in the North American monsoon region. J. Hydrol. 377, 59–70.
Milly, P.C.D., Dunne, K.A., 2016. Potential evapotranspiration and continental drying. Nat. Clim. Change 6, 946–949.
Morecroft, M.D., Woodward, F.I., 1990. Experimental investigations on the environmental determinations of δ13C at different altitudes. J. Exp. Bot. 41, 1303–1308.
National Oceanic and Atmosphere Administration. 2012. US climate division data plots (https://www.esrl.noaa.gov/psd/data/usclimdivs/).
Pallett, D.W., Pescott, O.L., Schäfer, S.M., 2016. Changes in plant species richness and productivity in response to decreased nitrogen inputs in grassland in southern England. Ecol. Ind. 68, 73–81.
Poncecampos, G.E., Moran, M.S., Huete, A., Zhang, Y., Bresloff, C., Huxman, T.E., Eamus, D., Bosch, D.D., Buda, A.R., Gunter, S.A., 2013. Ecosystem resilience despite large-scale altered hydroclimatic conditions. Nature 494, 349–352.
Qu, X., 2015. Temporal and spatial patterns of droughts for recent 40-year in Hulun Buir based on meterological drought composite index. Meteorol. Sci. Technol. 43, 103–107.
Rana, G., Katerji, N., 2000. Measurement and estimation of actual evapotranspiration in the field under Mediterranean climate: a review. Eur. J. Agron. 13, 125–153.
Ren, H., Xu, Z., Isbell, F., Huang, J., Han, X., Wan, S., Chen, S., Wang, R., Zeng, D.H., Jiang, Y., 2017. Exacerbated nitrogen limitation ends transient stimulation of grassland productivity by increased precipitation. Ecol. Monogr. 87, 457–469.
Scanlon, T.M., Kustas, W.P., 2012. Partitioning evapotranspiration using an eddy covariance-based technique: Improved assessment of soil moisture and land-atmosphere exchange dynamics. Vadose Zone J. 11, 811–822.
Schlesinger, W.H., Jasechko, S., 2014. Transpiration in the global water cycle. Agric. For. Meteorol. 189–190, 115–117.
Scott, R.L., Biederman, J.A., 2017. Partitioning evapotranspiration using long-term carbon dioxide and water vapor fluxes. Geophys. Res. Lett. 44, 683–6840.
Sun, Q., Miao, C., Duan, Q., 2017. Changes in the spatial heterogeneity and annual distribution of observed precipitation across china. J. Clim. 30, 9399–9416.
Sun, Y., Piao, S., Huang, M., Ciais, P., Zeng, Z., Cheng, L., Li, X., Zhang, X., Mao, J., Peng, S., 2016. Global patterns and climate drivers of water-use efficiency in terrestrial ecosystems deduced from satellite-based datasets and carbon cycle models. Glob. Ecol. Biogeogr. 25, 311–323.
Todd, S.W., Hoffer, R.M., Milchunas, D.G., 1998. Biomass estimation on grazed and ungrazed rangelands using spectral indices. Int. J. Remote Sens. 19, 427–438.
Trenberth, K.E., Dai, A., Schrier, G.V.D., Jones, P.D., Barichivich, J., Briffa, K.R., Sheffield, J., 2014. Global warming and changes in drought. Nat. Clim. Change 4, 17–22.
Vetter, S.H., Schaffrath, D., Bernhofer, C., 2012. Spatial simulation of evapotranspiration of semi-arid Inner Mongolian grassland based on MODIS and eddy covariance data. Environ. Earth Sci. 65, 1567–1574.
Vicente-Serrano, S.M., Beguería, S., López-moreno, J.I., 2010. A multiscalar drought index sensitive to global warming: the standardized precipitation evapotranspiration index. J. Clim. 23, 1696–1718.
Vicente-Serrano, S.M., Gouveia, C., Camarero, J.J., Beguería, S., Trigo, R., López-Moreno, J.I., Azorín-Molina, C., Pasho, E., Lorenzo-Lacruz, J., Revuelto, J., 2013. Response of vegetation to drought time-scales across global land biomes. Proc. Natl. Acad. Sci. U.S.A. 110, 52–57.
Vicente-Serrano, S.M., Schrier, G.V.D., Beguería, S., Azorin-Molina, C., Lopez-Moreno, J.I., 2015. Contribution of precipitation and reference evapotranspiration to drought indices under different climates. J. Hydrol. 526, 42–54.
Villegas, J.C., Espeleta, J.E., Morrison, C.T., Breshears, D.D., Huxman, T.E., 2014. Factoring in canopy cover heterogeneity on evapotranspiration partitioning: Beyond big-leaf surface homogeneity assumptions. J. Soil Water Conserv. 69, 78–83.
Vörösmarty, C.J., Federer, C.A., Schloss, A.L., 1998. Potential evaporation functions compared on us watersheds: possible implications for global-scale water balance and terrestrial ecosystem modeling. J. Hydrol. 207, 147–169.
Wang, L., Good, S.P., Caylor, K.K., 2015. Global synthesis of vegetation control on evapotranspiration partitioning. Geophys Res Lett 41, 6753–6757.
Wang, X., Guo, Y., He, J., 2014. Estimation of above-ground biomass of grassland based on multi-source remote sensing data. Trans. Chin. Soc. Agric. Eng. 30, 159–166.
Wang, P., Yamanaka, T., 2014. Application of a two-source model for partitioning evapotranspiration and assessing its controls in temperate grasslands in central Japan. Ecohydrology 7, 345–353.
Weaver, J.E., Albertson, F.W., 1939. Major changes in grassland as a result of continued drought. Bot. Gaz. 100, 576–591.
Wilske, B., Kwon, H.J., Long, W., Chen, S.P., Lu, N., Lin, G.H., Xie, J., Guan, W.B., Pendall, E., Ewers, B.E., 2010. Evapotranspiration (ET) and regulating mechanisms in two semiarid Artemisia-dominated shrub steppes at opposite sides of the globe. J. Arid Environ. 74, 1461–1470.
Wilson, T.B., Meyers, T.P., 2007. Determining vegetation indices from solar and photosynthetically active radiation fluxes. Agric. For. Meteorol. 144, 160–179.
Xu, L.K., Baldocchi, D.D., 2004. Seasonal variation in carbon dioxide exchange over a Mediterranean annual grassland in California. Agric. For. Meteorol. 123, 79–96.
Yang, Y., Wang, G., Wang, L., Yu, J., Xu, Z., 2014. Evaluation of gridded precipitation data for driving Swat model in area upstream of three gorges reservoir. PLoS One 9, e112725.
Yu, G.R., Wen, X.F., Sun, X.M., Tanner, B.D., Lee, X., Chen, J.Y., 2006. Overview of ChinaFLUX and evaluation of its eddy covariance measurement. Agric. For. Meteorol. 137, 125–137.
Zhang, N., Liu, C., 2014. Simulated water fluxes during the growing season in semiarid grassland ecosystems under severe drought conditions. J. Hydrol. 512, 69–86.
Zhang, Q., Liu, G., Hongbo, Y., Bao, Y., 2016. Temporal and spatial dynamic of ET based on MOD16A2 in recent four years in Xilin Gol steppe. Acta Agrestia Sinica 24, 286–293.
Zhou, S., Yu, B., Huang, Y., Wang, G., 2014. The effect of vapor pressure deficit on water use efficiency at the sub-daily time scale. Geophys. Res. Lett. 41, 5005–5013.
Zhou, S., Yu, B., Zhang, Y., Huang, Y., Wang, G., 2016. Partitioning evapotranspiration based on the concept of underlying water use efficiency. Water Resour. Res. 52, 1160–1175.